Mo70Cu30 composites synthesized by infiltration sintering and hot rolling with simultaneously improved mechanical and electrical properties

Fuxing Yao[a], Wenge Chen [a,*], Guangqing Lai[a], Jiangjiang Ma[a], Baojiang Ren[b], Xinwen Zhou[b], Ahmed Elmarakbi[c], Yong-Qing Fu[c]

[a] School of Materials Science and Engineering, Xi'an University of Technology, Xi'an, Shaanxi, 710048, P.R. China

[b] Metal Branch, Jinduicheng Molybdenum Co., Ltd., Xi'an 710060, China

[c] Faculty of Engineering and Environment, Northumbria University, Newcastle upon Tyne, NE1 8ST, UK.

*Corresponding authors: Prof. Wenge Chen

E-mail: wgchen001@263.net (W.G. Chen)

Abstract: In this study, Cu@Mo composite powders, prepared using an electroless plating method, were applied to synthesize Mo70Cu30 composites using infiltration sintering and hot rolling technologies. Microstructure, mechanical properties and physical properties of the synthesized Mo70Cu30 composites were studied. Results showed that the prepared Cu@Mo composite powders have a core-shell structure with Mo particles uniformly coated with Cu layers. Density values of Mo70Cu30 composites before and after the hot rolling process are 98.45% and 99.79%, their tensile strengths are 517 MPa and 753 MPa, and their thermal conductivities are 179.7 W/(m·K) and 214.6 W/(m·K), respectively. Formation of network Cu channels in the Mo70Cu30 composite is beneficial for achieving uniform microstructures, increased density, and enhanced thermal conductivity. Rolling process deforms the Cu phase into a fibrous shape, forming a good thermal conductivity channel and refining the Mo phase grains. The enhancement in the mechanical properties of the composites is attributed to the combined mechanisms of deformation strengthening and fine grain strengthening.

Keywords: Chemical plating; Mo70Cu30 composites; Rolling; Mechanical properties

1. Introduction

Molybdenum-copper (Mo-Cu) composite is a special composite material which combines high melting point, high hardness and low thermal expansion coefficient of molybdenum with high electrical and thermal conductivities and good ductility of copper. Due to its high thermal conductivity, low thermal expansion and superior mechanical properties, it is widely used in applications such as radiators and microwave absorbers in microelectronic packaging [1-8]. At present, the key research area for MoCu composites is how to improve both their mechanical and electrothermal properties.

Common preparation methods of MoCu composite materials include liquid phase sintering of MoCu mixed powders and liquid copper impregnation of molybdenum skeleton [9-12]. However, due to the large differences between the melting points of molybdenum and copper, their extremely low mutual solubility under equilibrium conditions, and the significant difference in their electronegativity (i.e., Mo=2.16, Cu=1.9), the MoCu composite materials prepared by the above traditional processes often show low density and poor mechanical and functional performance [3]. Recently preparation of composite materials using composite powders as raw materials is considered to be an effective method to improve both the mechanical and electrothermal properties of the composite materials [13]. For example, Wang et al. [14, 15] prepared copper-coated molybdenum composite powders using a heterogeneous precipitation and thermal reduction method, which effectively inhibited the aggregation of materials and growth of grains. The hardness, electrical conductivity and thermal conductivity of their prepared molybdenum copper composites reached 191.1 HV, 27.00 MS/m and 188.64 W/(m·K), respectively. Song et al. [16] prepared ultra-fine Mo-15wt.%Cu composite powders using a gel reduction method, and the conductivity of molybdenum-copper composite prepared using these composite powders reached 41.75% IACS and the Vickers hardness reached 300.15 HV. Zheng et al. [17] prepared W@Cu composite powder using a method of liquid mixing combined with hot gas reduction. The conductivity of WCu composite prepared using a 3D printing technology was as high as 96% IACS, and the relative density was 98.5%. However, so far, the strength and thermal conductivity of MoCu composites prepared by these methods are still far from the satisfactory values.

Deformation strengthening is one of the common strengthening methods, and is

often used to improve the mechanical properties of composite materials. In recent years, studies showed that large deformation has also a positive effect on the improvement of the thermoelectric properties of materials. For example, Wang et al. [18] prepared Mg-SiC/Cu composite materials using a cumulative rolling technology, and then studied effect of whisker orientation on the mechanical and thermal properties of the composite. Their results showed that when the composite has experienced a large plastic deformation, its hardness and strength have been increased by 60% and 41%. The number of conductive layers and thermal conductivity in this composite material have also been increased. Guo et al. [19] reported that thermal conductivity of CuCr30 composite for electrical contact materials has been increased by 50%. In the study of MoCu composite reinforced by plastic deformation, Zheng et al. [20] investigated the influences of different billet making processes on microstructures and properties of rolled MoCu sheets, and reported that the rolled molybdenum copper sheets prepared using the fusion method showed better thermal and electrical properties than those prepared using the mixed method, and the mechanical properties of the composite material were significantly improved after rolling.

Currently there are few studies on improving both the mechanical and electrothermal properties of MoCu composites using the Cu@Mo composite powders. Therefore, in this work, we prepared core-shell Cu@Mo composite powder using an electroless plating method. These powders were then used as raw materials to prepare MoCu composite material and improved the relative density of composite material by using a cladding rolling technology. To improve both the mechanical and electrothermal properties. The well-dispersed network of Cu strip was formed and enhance the electrothermal properties of MoCu composites, whereas the increased density and deformation strengthening mechanisms provided the good mechanical properties of the composites.

2. Experimental

2.1 Material and preparation process

Molybdenum powder with its purity > 98% and average particle size of 5 μm was provided by Xi'an Jinduicheng Molybdenum Industry Co., LTD. Pure copper powder with a purity of 99.9% and average size of 74 μm was provided by Beijing Xingrongyuan Co., Ltd. . Disodium ethylenediamine tetra acetic acid (EDTA-2Na) was provided by Tianjin Xinbaite Chemical Co., Ltd. Potassium and sodium tartrate (PST)

was obtained from Tianjin Damao Chemical Reagent Company. Copper sulfate pentahydrate ($CuSO_4 \cdot 5H_2O$) was obtained from Jinan Lebin Chemical Co., Ltd.

Preparation processes of Mo70Cu30 composites are illustrated in Fig. 1. Firstly, Cu@Mo composite powder was prepared using the electroless plating (see Fig. 1(a)). $CuSO_4 \cdot 5H_2O$ was used as the main solution for electroless copper plating, formaldehyde aqueous solution was used as the reducing agent, and EDTA-2Na and PST double complexing agent were used as the complexing agent. The detailed composition of the plating solution is listed in Table 1. Firstly, 10 g molybdenum powder was ultrasonically dispersed in the alcohol solution for 30 min, and then cleaned in NaOH 10~20 g/L and 35% HCl, for degreasing and surface roughening. In the electroplating process, NaOH was used to adjust the pH value of the solution to be 12~13, and the temperature of water bath was maintained at 60℃. The mixing speed was 300 r/min. The precipitates in the plating solution were filtered and washed with the deionized water, then dried in an oven for 2 h. They were then reduced in H_2 atmosphere at 500℃ for 90 min to obtain the MoCu composite powder.

Synthesis process of Mo70Cu30 composites is illustrated in Fig. 1(b). The composite powders were cold-pressed in a steel die at a pressure of 600 MPa and held for 10 s to obtain a compact of 12 mm×52 mm×10 mm. Then, the compact was placed in a graphite crucible, and the mass fraction of Cu in the MoCu composites was 30% with the addition of molten copper powder. The compact was sintered in a tube furnace under H_2 atmosphere with a heating rate of 8 ℃/min at 1350℃ for 90 min. At this temperature, fusion and sintering of powders improved the relative density of the composite [21] and ensured good mechanical and thermal properties [5].Finally, ZK-WS6 high-strength and large-distance rolling mill was used to hot roll the sintered parts. The rolling temperature was 750℃, and the single pass reduction was 10%. When rolled at this temperature, the Cu phase is in a dynamic recrystallization state, which could be deformed easily to enhance the sintering effect [22].

The line speed for rolling was 0.78 m/s. The single pass hot rolled sample was annealed at 400 ℃ for 10 min, and the rolling sample was annealed at 400 ℃ for 1 h after the rolling.

Table 1 Parameters and contents of electroless plating solution

Composition	Function	Concentration	Content (%)
CuSO4·5H2O	Main salt	20 g/L	27.8
HCHO	Reducing agent	20 ml/L	14.8
$NaKC_4H_4O_6$	Complexing agent	10 g/L	19.1
EDTA-2Na	Complexing agent	18 g/L	38.3
NaOH	pH regulator	150 ml/L (10%)	-

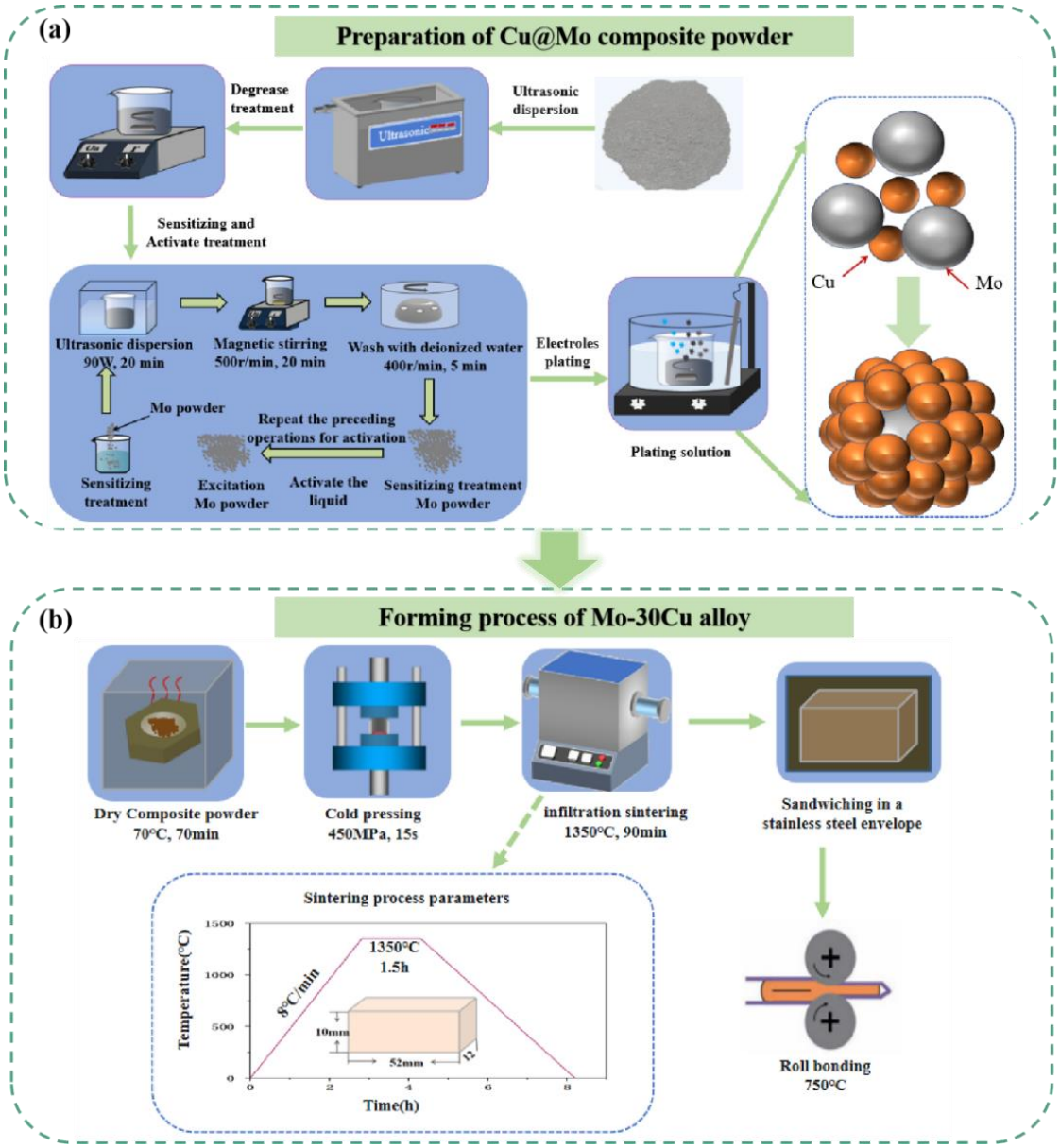

Fig. 1 Schematic illustrations of preparation process of Mo70Cu30 composites. (a) Cu@Mo composite powder preparation; (b) Preparation of Mo70Cu30 composites.

2.2 Characterization

Crystalline structure of Mo70Cu30 composites was determined using an X-ray diffractometer (XRD, XRD-7000S, Japan). The X-ray source material was Cu-Kα radiation, with the scanning speed of 8º/min, a scanning step of 0.02º, and a scanning two theta range of 10~90º. Microstructures of molybdenum powder, MoCu composite powder, MoCu composites and tensile fracture morphology of composites were observed using a scanning electron microscope (SEM, Zeiss Sigma) with an energy dispersive spectrometer (EDS). Texture, crystals and dislocations of rolled composites were analyzed using an electron backscattered diffraction (EBSD) analyzer (EDAX Hikari Plus, EDAX/OIM system 7.1). The acceleration voltage and current of EBSD were 20 kV and 13 mA, respectively, and the scanning step size is 0.1 μm. Microstructures of sintered and rolled composites were observed using an optical microscope (OM, OLYMPUS GX71) and an Image Pro Plus software were used to calculate the average grain size of sintered composites. The etching solution for the composite samples was a mixture of $FeCl_3$, HCl (20%) and alcohol (the ratio was 1:5:20), and the etching time was 30 s. A high-resolution transmission electron microscope (HR-TEM, JEM-3010) was used to characterize microstructures and interfacial structures of the composites. The relative density of MoCu composites was determined using the Archimedes principle. Micro-Vickers hardness tester (HV-120) was used to measure the microhardness of the material. Electrical conductivity of the materials was measured using a D60K digital metal conductance meter. Thermal conductivity of the material was measured using an LFA-427 thermal conductivity meter. Thermal expansion coefficient of the material composites in the temperature range of 25~450℃ was measured using Netzsch TMA 402F3 thermal expansion instrument.

3. Results and discussion

3.1 Microstructure Analysis

Fig. 2 shows the SEM images and particle size distributions of Cu@Mo composite

powder prepared using the electroless plating process. Fig. 2(a) shows the original Mo powder morphology, with sharp edges, smooth surface and uneven sizes. The particle size distribution of molybdenum powder is ranged from 0.4 to 10 μm (Fig. 2(b). The particle size of the powder is mostly concentrated within 3~6 μm, and the median diameter is 5.5 μm. Fig. 2(b) shows the morphology of Cu@Mo powder, in which small uniform spherical or dumbbell-shaped Cu particles are attached to the surface of Mo powder. The surface of Mo powder is completely coated with Cu, and the shape of the coated powder tends to be spherical. The median diameter of the Cu@Mo powder is 12.0 μm, and the powder size is significantly larger than that of the original Mo powder as shown in Fig. 2(a). Figs. 2(c) and 2(d) show the cross-section microstructure and line scanning distribution of the Cu@Mo composite powder. The outer element of a single powder particle is Cu, and the inner element is Mo, showing the formation of a core-shell structure. The thickness of Cu coating is about 0.8~1 μm. A transition layer with a thickness of about 0.2 μm was formed at the interfaces of Mo and Cu layers (see Fig. 2(d)). The thickness of the copper layer is closely related to the synthesis process, chemicals used and their concentrations, process time and temperature conditions. For example, Wang et al. [23] used the electroless plating method to prepare Cu@W composite powder with a formaldehyde solution as the reducing agent, and the obtained copper layer thickness was 0.91 μm.

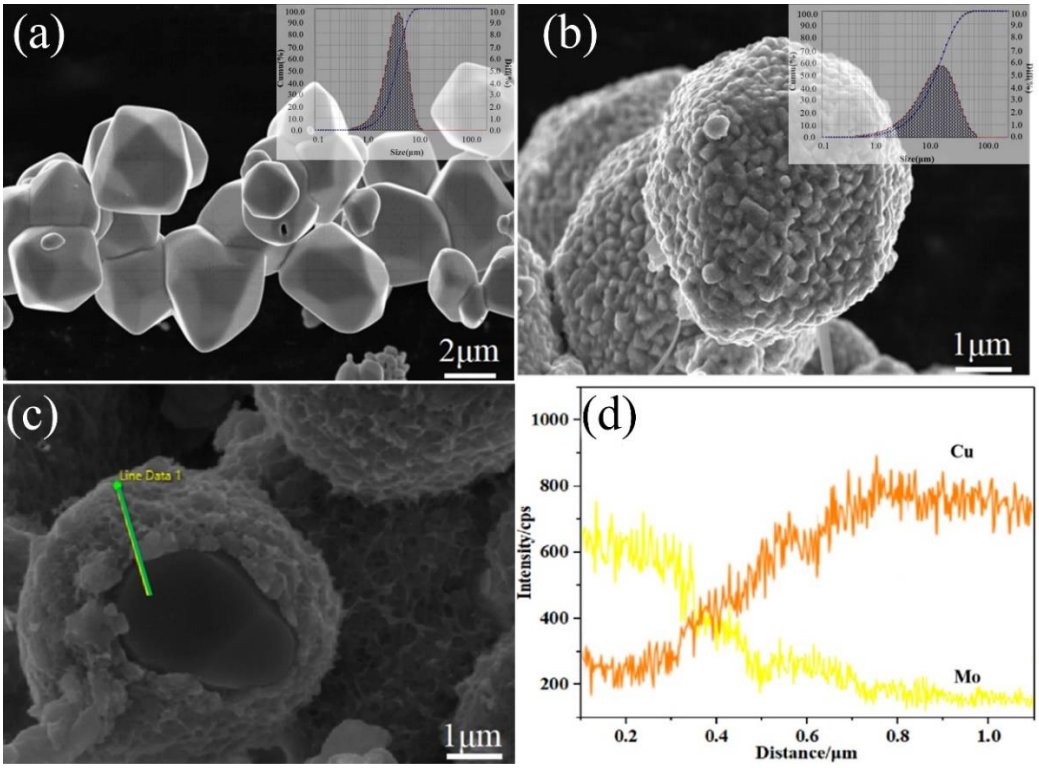

Fig. 2. SEM and EDS images of molybdenum powder before and after electroless plating. (a)

original molybdenum powder; (b) Cu@Mo composite powder; (c) cross-section of composite powder (d) EDS diagram of line1 in (c)

Fig. 3 shows the microstructure of the sintered and rolled Mo70Cu30 composites prepared by Cu@Mo composite powder. Fig. 3(a) shows the microstructure of sintered composites before corrosion. The yellowish Cu phase is evenly distributed in the gray molybdenum phase, and no other phases have been found in the microstructure. Fig. 3(b) shows the microstructure of sintered composites after etching. The corrosion object of etching solution is Cu, the remaining light-colored microstructure is Mo phase, and the dark-colored microstructure is Cu phase after etching. The Mo phase and Cu phase are uniformly distributed, and the Cu phase is wrapped around the Mo phase. There are no obvious defects of pores. This is because when the sintering temperature reaches 1350℃, there is a good "bonding" of Cu@Mo powder. The molten Cu phase flows inside the composites under the action of capillary force, thus improving the wettability of Mo particles in liquid copper. This makes the pores between particles fully filled with the liquid phase, thus reducing the porosity of the composites. At the same time, the coated Mo particles are rearranged under the action of surface tension, which improves the densification of the composites. The average grain size of the sintered composite is ~10.2 μm. The microstructures along the rolling direction (RD) and perpendicular to the rolling direction or transverse direction (TD) after hot rolling shown in Fig. 3(c) and 3(d) reveal that the Cu phase and Mo phase in the composites have different degrees of deformation after rolling. The Cu phase in the composites presents a fibrous morphology, whereas the Mo phase still shows the grain structure but the grain size of Mo phase is obviously refined. This is because Cu is an FCC crystal structure with multiple slip systems, and its deformation resistance is much smaller than that of Mo (which has a BCC structure with much less slip systems). Under the action of an extremal loading, the deformation rate of Cu is much higher than that of Mo. Therefore, the initial deformation of MoCu composites mainly occurs in the bonding phase of Cu. With the further increase of deformation, both Mo and Cu have shown a larger deformation. In addition, compared with the sintered composites, the grain size of rolled composites is reduced and the size uniformity is significantly improved.

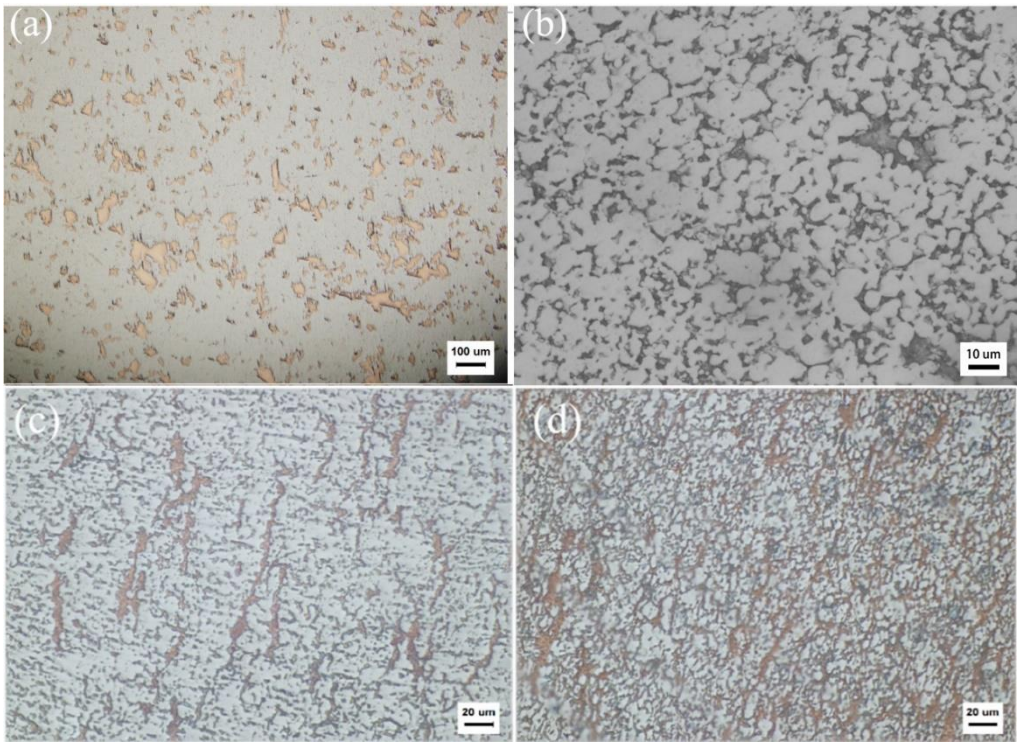

Fig. 3 Microstructure of sintered and rolled Mo70Cu30 composites (a) No corrosion sintered composites; (b) sintered composites corrosion; (c) along the rolling direction; (d) Perpendicular to the rolling direction.

Fig. 4 shows SEM images and EDS images of the sintered and rolled MoCu composites. It can be seen from Fig. 4(a) that the distribution of Mo and Cu phases of sintered composites is quite uniform, but there are a few micropores inside the composite material, mainly because some closed pores are not filled by liquid phase in the later stage of liquid phase sintering. This results in a small number of voids enclosed in the sintering body. Combined with EDS line map, it can be found that there is a transition layer with a thickness of about 0.5 μm in the sintered Mo and Cu phases of the composite. The formation of this transition layer can effectively improve the interface bonding strength and mechanical properties of the composite [24]. The EDS diagram shown in Figs. 4(b, c) reveals that Cu phase is distributed around Mo particles in a network pattern. This effectively forms Cu channels with good thermal conductivity inside the composite material and improves the thermal conductivity of the material. As can be seen from the SEM and EDS images of MoCu composite material after the rolling state in Figs. 4(d, e, f), the grain of the composite material is obviously refined after rolling, and flattened along the rolling direction. The defects such as pores are significantly reduced. The grain is obviously refined, and the Cu phases with long strips are distributed among Mo particles after rolling. These Cu

phases are closely bonded with Mo, which is conducive to improving the strength and density of the composite material. On the other hand, the dispersive distributed Cu phases can form thermally conductive channels, which can effectively reduce the obstruction of the grain boundary to the internal electron movement, thus improving both the electrical and thermal conductivities of the composite material [25].

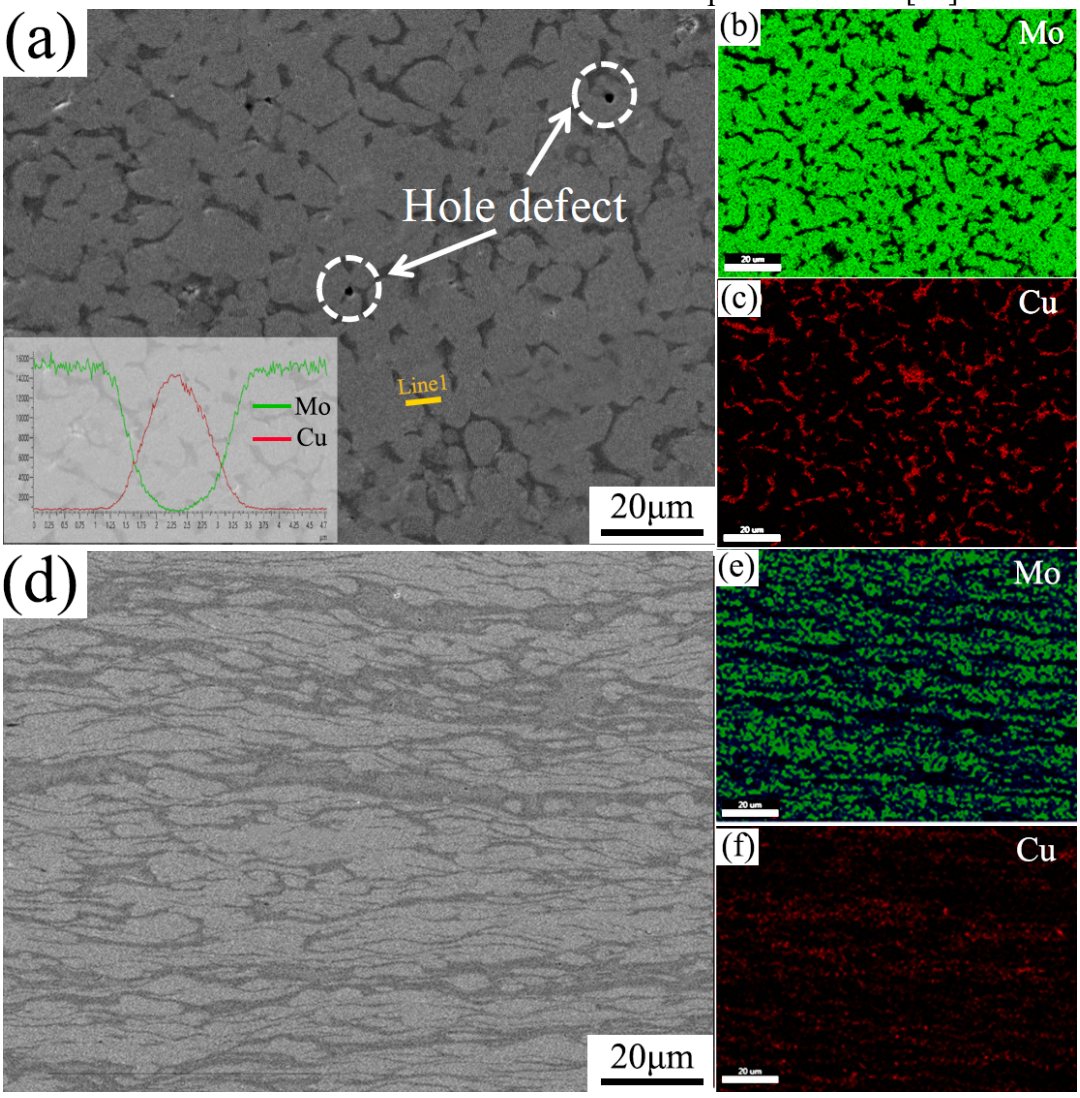

Fig. 4 SEM and EDS images of sintered and rolled MoCu composites: (a, b, c) sintered composites, (d, e, f) rolled composites.

Fig. 5 shows XRD patterns of Mo70Cu30 composites in sintered and post-rolled states. Only Mo and Cu diffraction peaks exist in both sintered and rolled states, and no other diffraction peaks appear, indicating that the composites are consisted of Mo and Cu phases. Compared with the sintered composites, the diffraction peak's intensity for the rolled composite is significantly reduced. Generally speaking, the broadening of diffraction peaks is a combined effect of grain refinement, micro-strain and instrument error [26]. Here, the peak broadening due to instrument error is negligible because the

results are all obtained using the same X-ray diffractometer. Therefore, the broadened diffraction peak of the rolled composites can be attributed to the grain refinement and micro-strain effect, both of which are contributed for the improvement of the mechanical properties of the composites. In addition, some of the diffraction peaks of the MoCu composite after rolling are shifted to the small angle direction, indicating that there were certain lattice distortion occurred after rolling, which contributes to the improved strength of the composite [27].

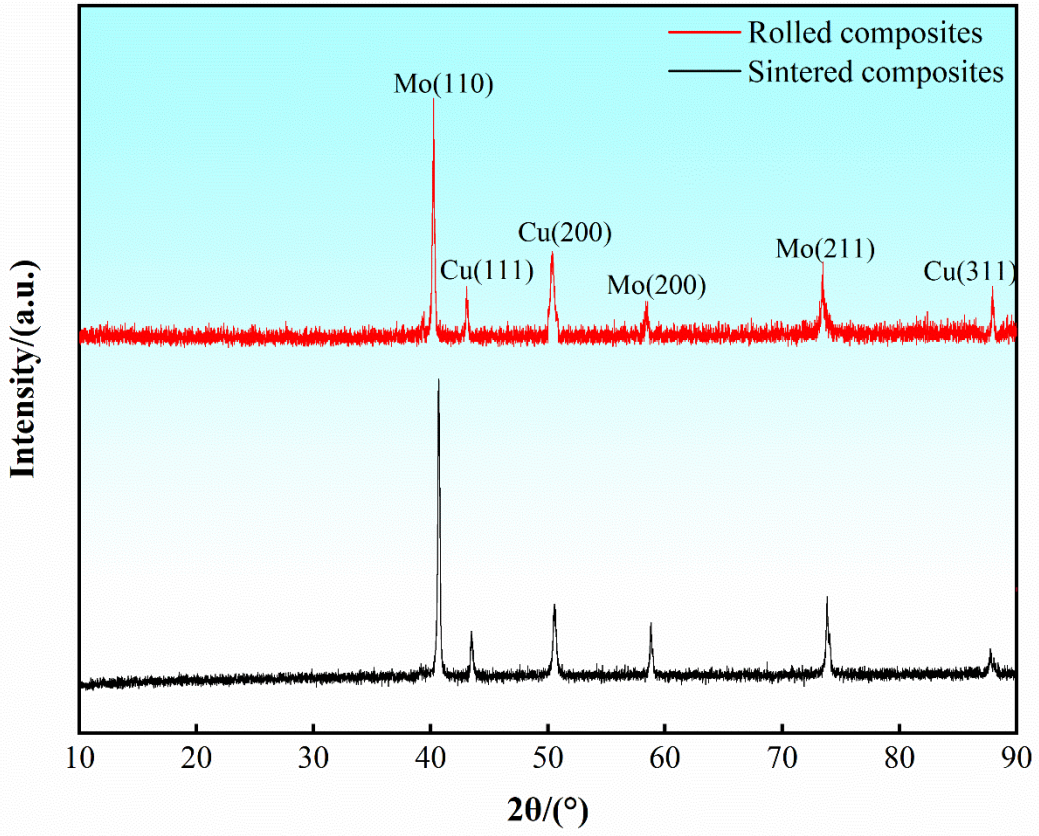

Fig.5 XRD patterns of the sintered and rolled Mo70Cu30 composites

Fig. 6(a) shows grain orientation distribution of Mo70Cu30 composites after rolling process. The microstructure of the rolled composites presents a mixed distribution of fine equiaxed grains and irregular coarse grains. Interestingly, the fine particles are mainly along Mo [101] and [111] orientations, indicating that their C-axis is largely deviated from the normal direction (ND) [28]. Moreover, the grains with [001] and [111] orientations show a fibrous morphology, and these regions are mainly Cu phases. Whereas the Mo phases are mainly fine grains, showing a preferred orientation of [101]. In addition, it can be seen from the grain size distribution diagram shown in Fig. 6(a) that the average grain size of the rolled composites is ~5.45 μm. If compared

with that of the as-sintered composites (~10.2 μm), it is significantly reduced. This reduction is grain size is helpful to improve the mechanical properties of the composites. As Cu in FCC is dominated by dislocation slip in the plastic deformation process, and the grains are stretched along the deformation direction, therefore, it shows a fibrous morphology. Whereas Mo with a BCC structure has a much less dislocation slip system, making it difficult for dislocations to slip, resulting in dislocation entanglement and blockage and storing a large amount of deformation energy [29]. This process will generate many substructures, and thus large grains have been separated into smaller grains.

Fig. 6(b) shows the representative pole figures of {110}, {100} and {111} plans for the rolled composites, in which RD is along the rolling direction, TD is along the vertical rolling direction, and ND is along the normal direction. The pole figure of {100} is a typical BCC metal rolling texture (with a TD offset texture feature). The strongest peak appears in the center of the pole diagram of {100}, and the maximum pole strength is estimated as 5.12. In the rolling process, the grain elongation of Cu occurs in the RD-ND plane [30], which causes texture formation of Cu phases. The texture distribution in the {110} pole figure shows that it is distributed along the RD direction, and the strongest peak of the polar graph is located along the RD direction. The maximum polar strength is 6.69, and is along the parallel orientation of the typical texture of face-centered cubic (FCC) metals [31]. The strongest peak in the {111} pole figure appears in the direction of ND deviation to RD of ±45°, and the second strongest peak is mainly aligned with the direction of TD, which is the typical texture of rolled BCC metal [32].

Fig. 6(c) shows the distribution diagram and statistical results of Low Angle Grain Boundaries (LAGB, 2~15°) and High Angle Grain Boundaries (HAGB, > 15°). The proportion of HAGBs in the composites is as high as 69.5%. This is because in the rolling deformation process, severe deformation leads to the rapid generation and movement of a large number of dislocations, and these dislocations are stacked during their movement in the composites. Therefore, many LAGBs are gradually formed in these locations. As the deformation is further increased, dislocations are accumulated at these LAGBs and then transformed into HAGBs [33]. On the other hand, after

annealing, some of the copper grains are recrystallized again, which increases the grain size and also the HAGBs. After rolling and annealing, the copper phase will partially recover and recrystallize, and the coarsening of sub-grains will be induced by the recovery. During the heat treatment process, the dislocations caused by the growth of sub grains will be increased, and the proportion of HAGBs in the material will be increased [34]. In addition, literature has shown that twin boundaries are easily formed in the Cu phase region when annealed at around 400℃ [35], which is also one of the reasons for the formation of HAGBs. However the recrystallization temperature of Mo is much higher at 1200℃ [36], so the recrystallization process is mainly dominated in the Cu phase. This is the main reason why the grains are still obviously refined after annealing. These HAGBs can act as a barrier for microcrack propagation, thereby increasing toughness and improving material's elongation [37]. In addition, the high density of dislocation entanglement and the formation of twinning structures will hinder the slip of the dislocations, thus improving the strength of the material.

Fig. 6(d) shows the Kernel-Average-Misorientation (KAM) diagram of the rolled Mo70Cu30 composites, which usually reflects the strain energy stored internally among grains and is used to estimate the dislocation density [38]. In general, the KAM value is closely related to the dislocation density, and the higher the KAM value, the higher the dislocation density [29]. It can be seen from Fig.6(d) that the calculated average KAM value of the composites after rolling is ~1.3, indicating that the dislocation density is quite high. This is mainly because the increase of geometric dislocations near the grain boundary can coordinate the deformation of the composites. The dislocation distribution is relatively uniform, mainly in the green area shown in Fig. 6(d). There are some fully recrystallized Cu phases in the blue region with a lower dislocation density and some partially crystallized Cu phase are seen in the red region with a higher dislocation density as shown in Fig. 6(a).

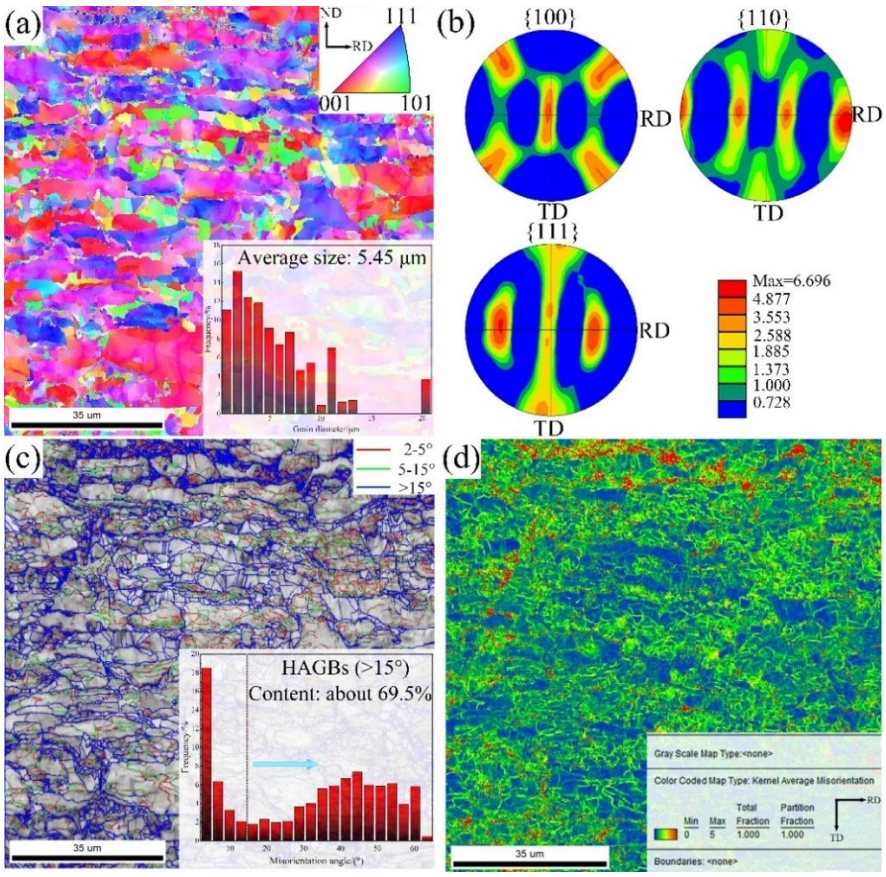

Fig. 6 EBSD results of rolled Mo70Cu30 composites (a) grain orientation diagram, (b) crystal face pole diagram, (c) orientation difference distribution diagram, (d) KAM map

Fig. 7 shows the HRTEM images of Mo70Cu30 composites after rolling process and the Fourier transform (FFT) diagram at the interface between Mo and Cu. From the diffraction pattern analysis shown in Figs. 7(a) and 7(b)), we can identify that the Cu phase (FCC structure) and the Mo phase (BCC structure) are the gray area (region I) and gray-black areas (region III), respectively. An interfacial reaction layer with a width of about 2.5 nm was formed between the Mo and Cu phases, which enhances the grain boundary strength [39], and numerous dislocations were piled up in the Mo phase (see the white circle in Fig. 7(a)). This is because stress sensitivity index of Mo (with a BCC structure) is small. Although many dislocations are generated under the severe plastic deformation, they are difficult to slip, thus forming dislocation entanglement [36]. As shown in the HRTEM image of region I in Fig. 7(b), the twin boundaries appear in the Cu phase region. Twining is a typical plastic deformation mode of materials, and is usually completed by the macroscopic strain generated by twin dislocation (TDs) slip [40]. In this study, it can be seen from the grain orientation diagram shown in Figure 6(a) that there are large differences in the structure orientation of twins in composite materials, and there are twins with multiple orientations. Combined with Figure 6(c), it

is found that the content of large Angle grain boundaries near 60° is high, which is a typical characteristic of annealing twins [41].

It can be seen from the grain orientation diagram shown in Fig. 6(a) that there are large differences in the structure orientation of twins in the composite materials, and there are twins with multiple orientations. Combined with Fig. 6(c), it is found that the content of HAGBs near 60° is relatively high, which is a typical characteristic of annealing twins [41]. Following are the causes of twin formation:

(1) Deformation storage can promote the generation of Shockley partial dislocations and the formation of Cu phase annealing twins in the FCC Cu structure [42]. The dislocations generated by a high strain rate deformation are evenly distributed and small dislocation cells are formed, which hinders the dislocation rearrangement and dynamic recovery process. Therefore, the dislocation density in the deformed matrix is higher. The higher the storage energy of Cu in the rolling deformation process, the higher the storage energy, which can promote the generation of Shockley partial dislocation, and thus promote the formation of annealing twins [43, 44].

(2) Dynamic recrystallization promotes the formation of twins. Cu is a face-centered cubic structure crystal with middle and low fault energy, and the deformation process is mainly dominated by dislocation slip, and the slip system is {111}[110], dislocation slip is first formed as [111] orientation (see Fig. 5) [45]. With the increased deformation, the distortion energy stored in plastic deformation and the thermal state of the composite during rolling deformation jointly promote the partial recovery and recrystallization of the material, and then induce the generation of twins [46]. On the other hand, under a high temperature rolling deformation, the sample is subjected to rolling pressure and roll friction during deformation, and deformation heat induced twinning easily occur under the action of composite stress [47].

(3) Driving of rolling internal stress. After a large deformation of the material, there is a large amount of residual stress in the grains, which provides sufficient driving force for GB migration [48], and thus increases the formation probability of Cu phase annealing twins.

(4) {111} atomic stacking misalignment. Because the FCC structure of Cu has the lowest stacking fault energy in {111}. Atomic stacking faults often occur in {111} during annealing, and dislocation damage has been introduced into the material after rolling deformation. This makes it easy to generate additional {111} steps along the grain boundary as the slip dislocation propagates across the grain boundary [49]. The

step creates Shockley partial dislocations near the grain boundary, which repel each other and slip out of the boundary, thus producing the twins [42].

Under the action of Peach-Koehle force in a small range, these ITBs move and produce twinning structures through a stop-start-moving-drag partial dislocation mechanism [50].

Figs. 7(c) and 7(d) are FFT and IFFT results of the yellow box in Fig. 7(a), respectively. After calibration, there are two kinds of lattice fringes at the interface of Mo and Cu phases (region II). The spacing of lattice fringes is 0.160, which is similar to the spacing of Mo (200) crystal faces. The lattice fringe spacing of 0.212 is similar to that of Cu (111) crystal faces. This indicates that Mo70Cu30 composite has no dynamic re-precipitation to produce the second phase after rolling, which is consistent with the results of XRD analysis. By calculating the lattice mismatch between Mo and Cu, the orientation relationship between them can be obtained. The calculation formula is shown in equation (3) [51].

$$\delta = \frac{d_2 - d_1}{d_1} \quad (3)$$

where δ is the lattice mismatch degree; d_2 is the crystal plane spacing of Cu (111). d_1 is the crystal plane spacing of Mo (200) (see Fig. 7(d)). The calculated mismatch between these two values is ~32.5%. Combined with Fig. 7(c), it is proved that the interface of molybdenum phase and copper phase is non-coherent.

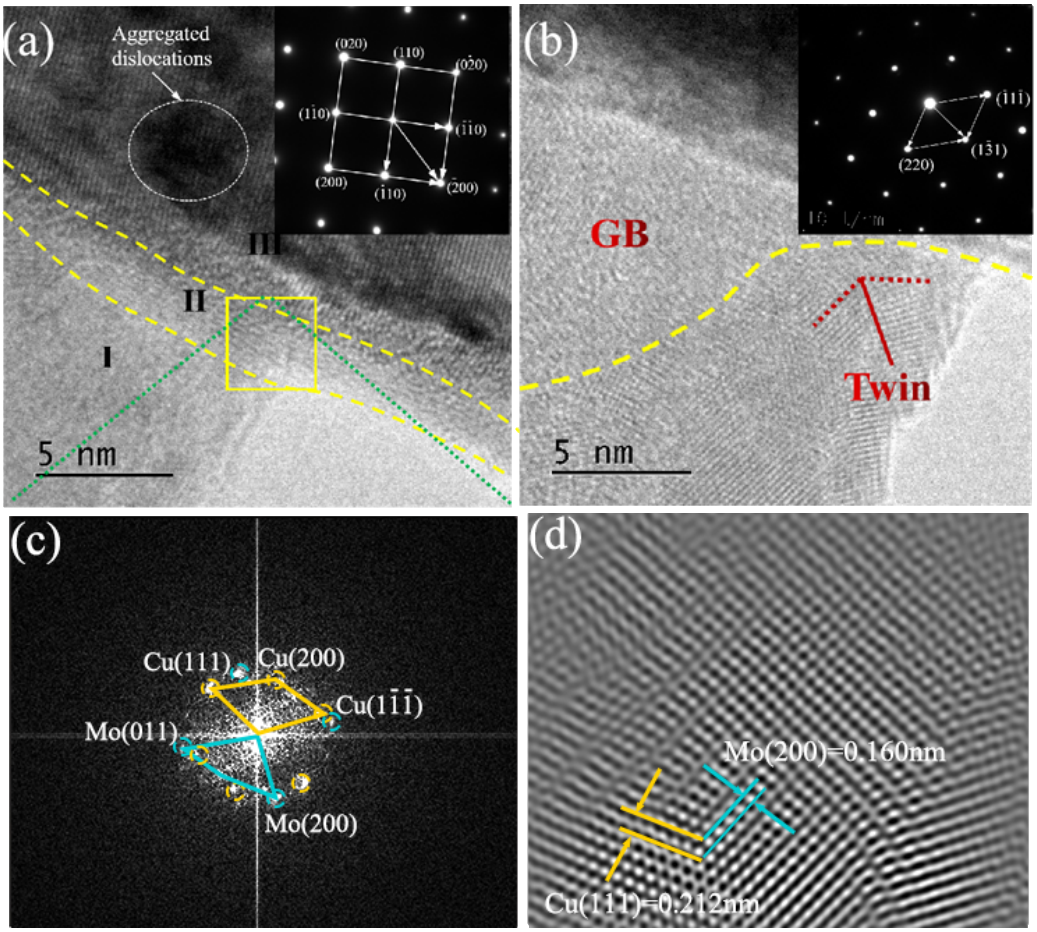

Fig. 7 HRTEM, FFT and IFFT images of rolled composites. (a) high-rate HRTEM; (b) high-magnification HRTEM; (c) FFT in yellow box in (a); (d) IFFT in yellow box in (a).

Fig. 8 shows a schematic diagram of the rolling deformation process of Mo70Cu30 composites. During the rolling process, the grain orientation is gradually shifted along the rolling direction. The changes of grain morphology and sizes can be divided into three regions, i.e., before rolling (region I), during rolling deformation (region II) and after rolling (region III). Region I is less affected by the rolling force, and the shapes of grain are almost unaffected. The structure is complete, and the grain is randomly oriented. Zone II is a rolling stress concentration zone, or a plastic deformation zone. In the unidirectional rolling state, the grain is subjected to stress along both the rolling direction and transverse rolling direction. With the applied stress, the Cu phase with an FCC structure has multiple slip systems, and the plastic deformation is mainly controlled by the slip movement of dislocations and the formation of twins [52]. A fibrous Cu phase structure is formed along the rolling direction. On the other hand, the dislocations in the Mo phase of BCC structure is not easy to slip due to its high stacking fault energy [53]. During dislocations' movement under stress, various phenomena such as dislocation cutting and entanglement can occur and thus restrict the further

movement of the dislocation. These will increase deformation resistance and improve the strength of the materials [54]. Region III is the rolling completion zone. The grain in this region has experienced a large plastic deformation. The fibrosis structure of Cu phase forms a certain preferred orientation, and the Mo phase forms many sub-grain boundaries, resulting in obvious grain refinement effect.

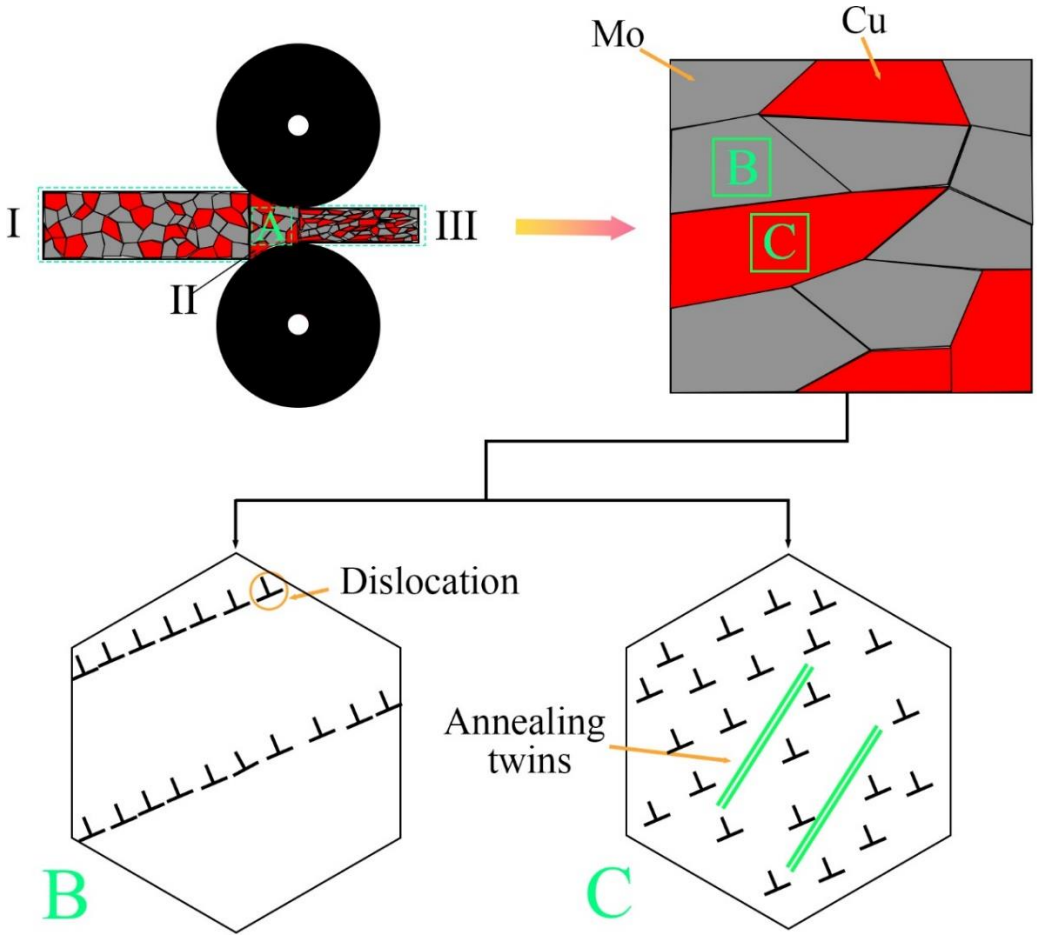

Fig. 8 Schematic diagram of Mo70Cu30 rolling process and microstructure change

3.2 Performance Analysis

Fig. 9(a) shows the engineering stress-strain curves of the sintered and rolled Mo70Cu30 composites. Both sintered and rolled Mo70Cu30 composites contain three deformation stages, i.e., elastic deformation stage, uniform plastic deformation stage and fracture stage. This indicates that the Mo70Cu30 composites have typical elastic/plastic deformation characteristics. The strength of the rolled composites is obviously higher than that of the sintered composites, but the ductility is reduced as shown in Fig. 9(b). Compared with the as-sintered Mo70Cu30 composites, the ultimate tensile strength of rolled composites is increased by about 45%, up to 753 MPa, and the yield strength is increased by about 70%. At the same time, compared with the

elongation of the sintered Mo70Cu30 composites (18.9%), that of the rolled composites elongation is reduced, but it can still be maintained at ~15%. The improved mechanical properties of the rolled composites is mainly attributed to the reduction of internal defects such as holes and the improvement of microstructure's uniformity [55], and the refined microstructures due to the dynamic recrystallization during the rolling process [56]. According to the Hall-Page relationship, formation of fine recrystallized grains helps to improve the strength [57].

If compared with the rolled Mo30Cu composites prepared using the other methods such as liquid phase sintering [58], the rolled Mo70Cu30 composites prepared in this study shows higher ultimate tensile strength and larger elongation (see Table 2). This indicates that under the same deformation, Mo70Cu30 composites prepared by Cu@Mo composite powder can effectively improve the strength and ductility of Mo70Cu30 composites. This is mainly affected by the preparation process of the composite material. The preparation of MoCu composite using the Cu@Mo composite powders can shorten the diffusion and homogenization time, avoid grain growth and component segregation, and thus show more uniform plastic deformation. When the MoCu composites is prepared by Cu@Mo composite powder, Cu particles are uniformly coated on the surfaces of Mo particles, which achieves the uniform dispersion of Cu phase during sintering. The uniform dispersion of Cu phase can effectively avoid large stress concentration in the deformation process of the composites, thereby improving its elongation. On the other hand, the larger the deformation during rolling process, the better the grain refinement effect. The grain refinement not only hinders the dislocation movement, but also uniformly disperses the stress in the deformation process, and ultimately improves the strength and ductility of the sample [59].

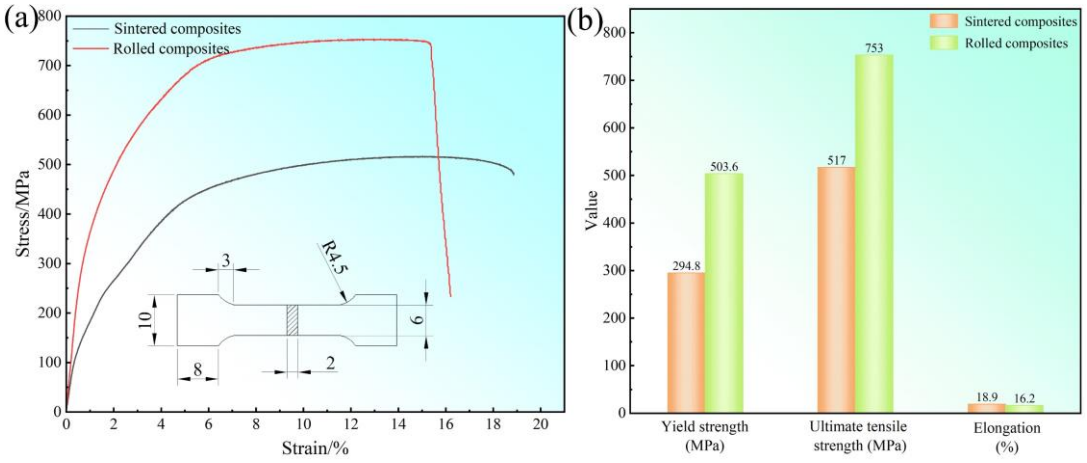

Fig. 9 Tensile properties of sintered and rolled Mo70Cu30 composites: (a) stress-strain curve, (b)

tensile properties.

Table 2 Comparison of properties of rolled Mo70Cu30 composites

Materials	Yield strength (MPa)	Tensile strength (MPa)	Rate of elongation (%)	Reference
Mo70Cu30	503.6	753	16.2	This work
Mo70Cu30	492	619.6	15.9	[20]
Mo70Cu30	513.6	640.4	14.3	[20]

Fig. 10 shows SEM images of tensile fracture morphology of Mo70Cu30 composites in both sintered and rolled states. As can be seen from Fig. 10(a), the sintered MoCu composite shows a large number of dimples and holes (as shown in the red circle in Fig. 10(a)), and the Cu phase shows a large plastic deformation and tearing phenomenon. At a higher magnification (see Fig. 10(b)), the composites have shown uniform distribution of two phases and a Cu-coated Mo structure. The evenly distributed network structures of W and Cu are beneficial to the improvement of mechanical properties, electrical conductivity and thermal conductivity of Mo-Cu composites [14]. There is no obvious plastic deformation of Mo particles in the fractured surface, and the fracture morphology is smooth, showing a typical trans-granular fracture mode. This is because Cu has an FCC structure with a good ductility at room temperature, whereas Mo has a BCC structure and is brittle. Therefore, the fracture of Mo-Cu sintered composite appears as a brittle fracture of Mo matrix. However, the Cu phase is ductile fracture after plastic deformation [60]. These mixed fracture modes are closely related to the good strength and ductility of the obtained Mo-Cu composites.

As seen from Figs. 10(c) and 10(d), compared with the sintered state, the numbers of plastic dimples and pores for the rolled Mo70Cu30 composites are reduced, and the size of the dimples is significantly reduced. At the same time, some tearing edges are observed, indicating that the composites have a good ductility. The fracture surface is relatively smooth, and the brittle fracture phenomena become more significant. These lead to the increase of strength of the composites and decreased of ductility.

Based on the results, the fracture mechanisms of the sintered and rolled Mo70Cu30 composites can be summarized as follows. When the sintered composites are stretched, cracks are originated from the holes or other defects formed during sintering. Under the action of external forces, a large stress concentration is easily generated at the micropores in the composites, resulting in the initiation of cracks. With further

increased stress, these cracks will spread along the Mo-Cu interfaces to the composite's surface until the Mo and Cu phases are completely fractured. However, when the rolled composites are stretched, due to the reduction of internal micro-holes under the rolling action, the grain structure is refined. The wettability between Mo and Cu is also improved after annealing and the interfacial bonding strength is thus improved. After the external tension, the fracture of the sample begins at the Mo particle, and finally the sample suddenly breaks.

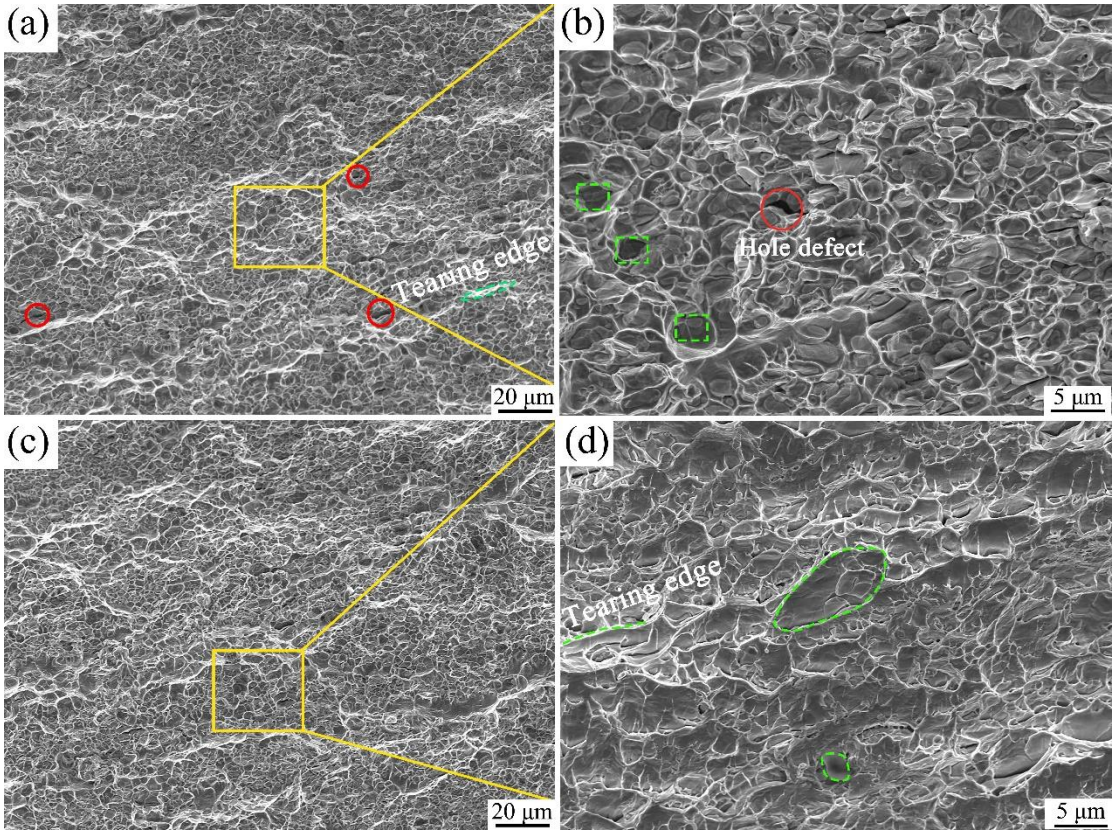

Fig. 10 Tensile fracture morphology of sintered and rolled Mo70Cu30 composites: (a, b) sintered composites, (c, d) rolled composites

Fig. 11 shows Coefficient of Thermal Expansion (CTE) results of Mo70Cu30 composites. The initial testing temperature is 25℃. When the temperature is increased from 25℃ to 450℃, the TECs of the rolled composites are significantly reduced compared with those of the sintered composites. This is mainly due to the rolling deformation which enhances the interfacial bonding of Mo and Cu phases and refines of the grains. However, the changing trends of TEC for these two phases are similar, which decreases from 11.3×10^{-6} /K to 7.67×10^{-6}/K and from 9.93×10^{-6} /K to 6.59×10^{-6} /K, respectively, both of which are far lower than the coefficient of thermal expansion of copper matrix [61] (17.70×10^{-6} /K). The TEC results can meet the requirements of electronic packaging materials.

The change of the CTEs of the composites can be divided into three stages, i.e., the sharp decrease of stage I (25 ~ 50℃), the smooth transition of stage II (50 ~ 150℃) and the slow decrease of stage III (150 ~ 450℃). The generation of this change trend is related to the elastic-plastic deformation of the material. The elastic strains of Mo and Cu contribute to the overall expansion behavior [22]. The CTE of Mo in MoCu composites is not sensitive to temperature, and the CTE of the composites is mainly controlled by the CTE of Cu at the testing temperature [50]. Because the core-shell structure of Cu@Mo powder reduces the bonding between Mo particles, the ability of Mo phase to inhibit the expansion of the composites has been weakened at the initial temperature, and thus the composites show a high CTE of copper phase. However, with the gradual increase of temperature (stage I), the thermal expansion rate decreases rapidly due to the low expansion of Mo, which causes the rapid decrease of CTE. With the further increase of temperature (stage II), the copper phase (in compressive stress) and molybdenum phase (in tensile stress) are both in an elastic state, and the copper phase has an elastic strain. However, due to the high elastic modulus of Mo, the elastic strain is small within this temperature range. In stage III, the copper phase has plastically deformed and no longer shown elastic deformation. During thermal expansion, Cu is in the form of plastic deformation, and the Mo phase is still in an elastic state, therefore, the elastic modulus of Mo decreases slightly with the increase of temperature, and elastic strains are gradually increased. In this stage, the expansion of Mo phase is dominant. However, as the thermal expansion coefficient of Mo itself is relatively small, the CTE of the composites decreases continuously. When the temperature is about 400℃, the recrystallization of copper occurs, and the increase rate of grain size decreases and thermal expansion is also decreased.

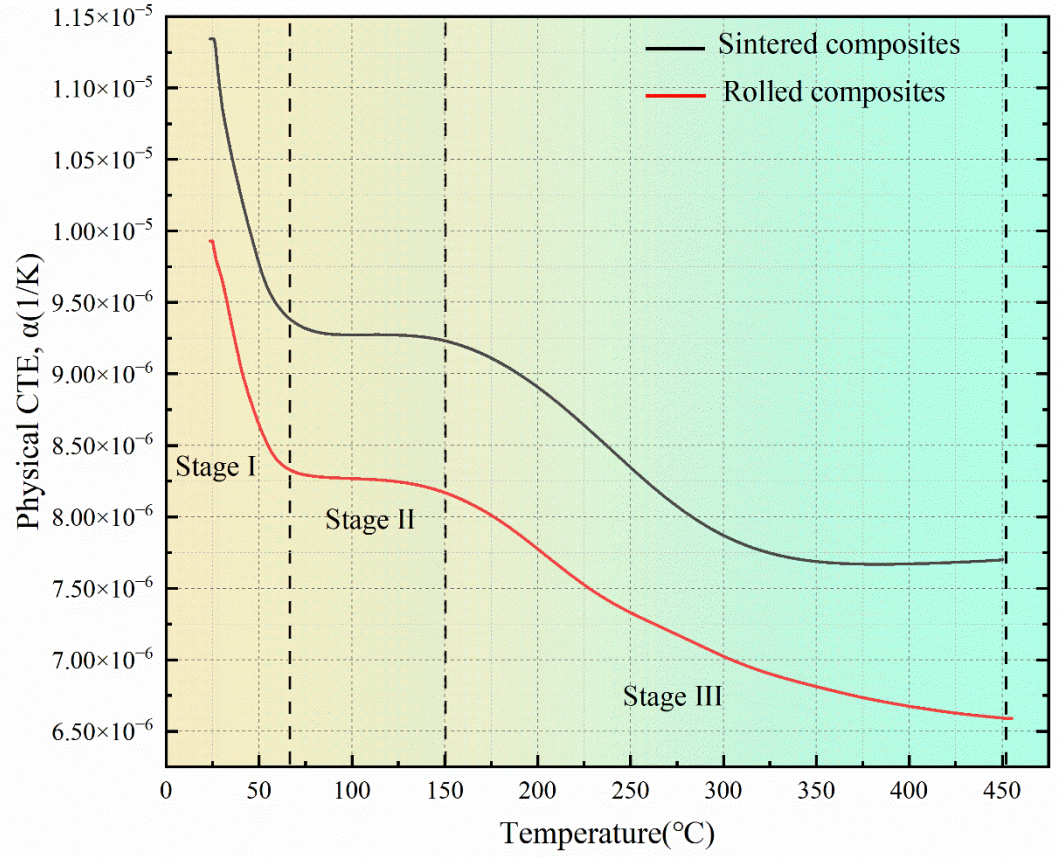

Fig. 11. Thermal expansion coefficient curves of Mo70Cu30 composites in sintered and rolled state

Fig. 12(a) shows the obtained results of density, hardness, conductivity and thermal conductivity for the sintered and rolled Mo70Cu30 composites. Most of the properties of Mo70Cu30 composites in the rolled state are significantly improved compared with those in the sintered state. For example, the sintered Mo70Cu30 composites has a density of 98.45%, a conductivity of 45% IACS, a thermal conductivity of 179.7 W/(m·K), and a hardness of 179.47 HV. By contrast, the density of the rolled Mo70Cu30 composites is only increased by 1.34% if compared to that of sintered one. The electrical conductivity and thermal conductivity are increased by 8.6% and 19.4%, respectively, and the hardness is increased by 39.2%.

If compared with the MoCu composites prepared by the traditionally mixed MoCu powder sintering method, the sintered composites prepared in this study using the Cu@Mo composite powder sintering shows a relatively higher density. For example, the density of Mo70Cu30 composites prepared by Zhang et al. [6] using ultra-fine molybdenum powder as raw material and sintered at 1200℃ is 97.45%. The density of Mo-25Cu composites prepared by Sun et al. [62] using MoCu nano-powder sintered at 1200℃ was 97%. The relatively high density achieved in this study is related to the

unique core-shell structure of Cu@Mo composite powders and the high sintering temperature in this study. During the sintering process, when the temperature exceeds the melting point of copper (1083℃), liquid phase copper are connected to form a bridging copper network throughout the entire structure, which can effectively improve the densification of the composites [63]. The core-shell structure of Cu@Mo powder improves the formation of the copper network distribution and enhances the bonding of Cu phase, and enhances the densification of the composites. At the same time, the increase of density can enhance the interface bonding strength, thus improving the thermal and conductive properties of the material [64]. This is the main reason why the electrical and thermal conductivities of the rolled composites are significantly higher than those of the sintered composites. In general, the increase of relative density means the decrease of porosity in the sample, resulting in higher hardness of the composite material [65]. However, the higher sintering temperature will cause the volatilization of the copper phase, resulting in formation of some micropores, and the decreased thermal and electrical conductivities of the composites [62].

Due to the large plastic deformation occurring in the rolling process, the rolled samples have a higher dislocation density and achieve a grain refinement effect, and the hardness of the materials is significantly increased under the joint action of deformation strengthening and fine grain strengthening [29, 66].

Thermal conductivity is a key fundamental characteristic of composite materials. Density, grain size, grain boundaries, or the second phase, all will significantly affect the thermal conductivity of the material [67]. The thermal conductivity and electrical conductivity are positively correlated. In this study, there is a significant enhancement of the thermal conductivity of the composites by rolling, which can be attributed to the following reasons.

(1) The first reason is the increase in density. Generally speaking, rolling refines the grain size of the sample, thus increasing the grain boundary, which will hinder the electron diffusion and reduce the conductivity and thermal conductivity of the material [68]. However, at the same time, the rolling deformation eliminates the defects such as micropores in the sintered sample. The porosity of the sample is reduced, thus a complete electron migration channel could be formed in the composites, which greatly improves the transportation of electrons. Therefore, the reduction of porosity will greatly improve the thermal conductivity of the material [69].

(2) Rolling reduces the number density and weakens the interfacial scattering of

electrons, thus increasing the thermal conductivity [70];

(3) Point defects in grains are eliminated in the rolling process and electron scattering is reduced, thus improving electron thermal conductivity [71].

Fig. 12(b) compares the comprehensive properties (hardness and thermal conductivity) of the Mo-Cu composites prepared in this study with those prepared by other different methods from literature. The rolled Mo70Cu30 composites prepared in this study has significantly improved thermal conductivity of the composites with higher hardness and better comprehensive properties.

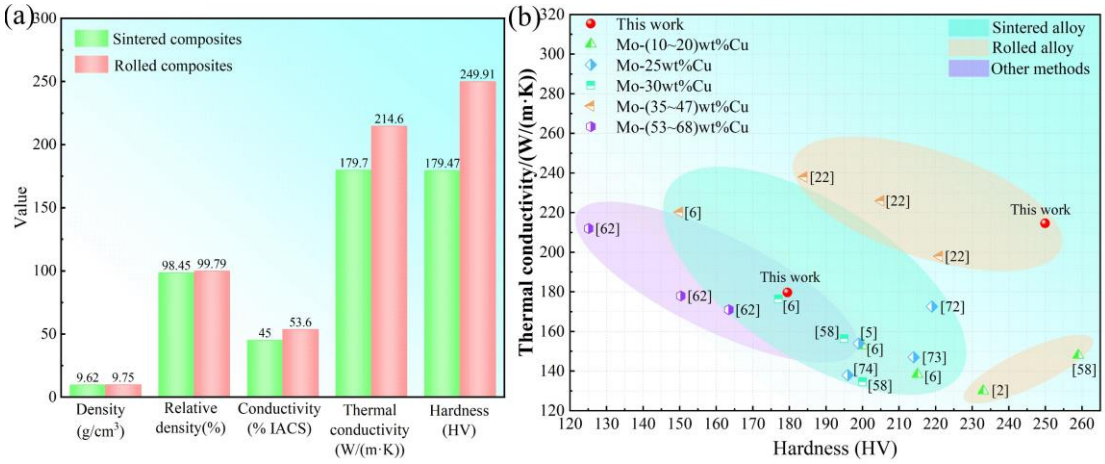

Fig. 12 Basic properties of sintered and rolled Mo70Cu30 composites. (a) Bar chart of density, electrical conductivity, thermal conductivity and hardness, (b) Comparison of properties of Mo-Cu composites with different preparation techniques [2, 5, 6, 22, 58, 62, 72-74]

4. Conclusion

In this study, effects of Cu@Mo composite powder and rolling process on the microstructure and properties of Mo70Cu30 composite were investigated, and the enhancement mechanisms were studied. The following conclusions were obtained from this study.

1. Core-shell composite powders with high sphericity, uniform particle size was prepared using copper plating process. Cu@Mo composite powder with unique core-shell structure was dispersed uniformly in Mo70Cu30 composites, forming a good copper thermal conductivity channel. After rolling, grain refinement effect is significant with few porosity and other defects, and the mechanical and thermal conductivity are improved.

2. In the rolling deformation process of Mo70Cu30 composites, due to the difference slip mechanisms of Mo and Cu phases, dislocation entanglement is formed in the Mo phase which promotes the grain refinement. The Cu phase generates plastic

deformation with dislocation slip and twins, thus forming a fibrous structure in the rolling direction.

3. In the process of tensile fracture, the as-sintered composites with the internal micropores and poor interfacial bonding show a brittle fracture of Mo phase and ductile fracture of Cu phase. The rolled composites have a better interfacial bonding of Mo and Cu phases, thus preventing the crack propagation or generation in the Mo matrix and resulting in increased strength.

Acknowledgements

The authors would like to acknowledge the financial supports from Key Research and Development Projects of Shaanxi Province (No. 2020ZDLGY12-06), Science and Technology Project of Xi'an City (No.2022JH-ZCZC-0048) and (No. 23ZDCYJSGG0042-2022).

Reference

[1] Z.U. Arif, M.Y. Khalid, A. Al Rashid, E. ur Rehman, M. Atif, Laser deposition of high-entropy alloys: A comprehensive review, Optics & Laser Technology 145 (2022) 107447. https://doi.org/https://doi.org/10.1016/j.optlastec.2021.107447

[2] X.-P. Ji, W.-C. Cao, C.-Y. Bu, K. He, Y.-D. Wu, G.-H. Zhang, A new route for preparing Mo-10wt.%Cu composite compacts, International Journal of Refractory Metals and Hard Materials 81 (2019) 196-205. https://doi.org/https://doi.org/10.1016/j.ijrmhm.2019.03.008

[3] J.L. Johnson, Activated liquid phase sintering of W–Cu and Mo–Cu, International Journal of Refractory Metals and Hard Materials 53 (2015) 80-86. https://doi.org/https://doi.org/10.1016/j.ijrmhm.2015.04.030

[4] L.-M. Luo, X.-Y. Tan, Z.-L. Lu, X.-Y. Zhu, X. Zan, G.-N. Luo, Y.-C. Wu, Sintering behavior of W–30Cu composite powder prepared by electroless plating, International Journal of Refractory Metals and Hard Materials 42 (2014) 51-56. https://doi.org/10.1016/j.ijrmhm.2013.10.012

[5] B. Li, H. Jin, F. Ding, L. Bai, F. Yuan, Fabrication of homogeneous Mo-Cu composites using spherical molybdenum powders prepared by thermal plasma spheroidization process, International Journal of Refractory Metals and Hard Materials 73 (2018) 13-21. https://doi.org/https://doi.org/10.1016/j.ijrmhm.2018.01.022

[6] H. Zhang, W.-C. Cao, C.-Y. Bu, K. He, K.-C. Chou, G.-H. Zhang, Sintering behavior of molybdenum-copper and tungsten-copper alloys by using ultrafine molybdenum and tungsten powders as raw materials, International Journal of Refractory Metals and Hard Materials 88 (2020) 105194. https://doi.org/10.1016/j.ijrmhm.2020.105194

[7] W. Zhang, L. Chen, C. Xu, W. Lu, Y. Wang, J. Ouyang, Y. Zhou,

Densification, microstructure and mechanical properties of multicomponent (TiZrHfNbTaMo)C ceramic prepared by pressureless sintering, Journal of Materials Science & Technology 72(13) (2021) 23-28.

[8] J.L. Johnson, D.F. Heaney, N.S. Myers, 23 - Metal injection molding (MIM) of heavy alloys, refractory metals, and hardmetals, in: D.F. Heaney (Ed.), Handbook of Metal Injection Molding (Second Edition), Woodhead Publishing2019, pp. 535-573.

[9] Y. Xia, Y.Q. Song, S. Cui, C.G. Lin, S.L. Han, Preparation and properties of Mo-Cu and W-Cu alloys, Chinese Journal of Rare Metals 32(002) (2008) 240-244.

[10] L. Xu, C.Zhang, LiboYan, MiPeng, JinhuiXia, HongyingGuo, Shenghui, Fabrication of tungsten-copper alloys by microwave hot pressing sintering, Journal of Alloys and Compounds: An Interdisciplinary Journal of Materials Science and Solid-state Chemistry and Physics 658(Null) (2016).

[11] Li, Chenguang, Zhou, Yihan, Xie, Yuehuang, Dengshan, Zhang, Deliang, Effects of milling time and sintering temperature on structural evolution, densification behavior and properties of a W-20wt.%Cu alloy, Journal of Alloys and Compounds: An Interdisciplinary Journal of Materials Science and Solid-state Chemistry and Physics (2018).

[12] Y.-W. Cho, J.-J. Sim, J.-S. Byeon, T.-S. Kim, K.-A. Lee, H.-J. Ju, S.-J. Seo, K.-T. Park, Comparative Study of the Properties of Cu-Cr-Mo System Electrical Contact Material by Sintering and Infiltration Methods, Metals 11(5) (2021) 700. https://doi.org/10.3390/met11050700

[13] R.M. Mohamed, Characterization and catalytic properties of nano-sized Pt metal catalyst on TiO2-SiO2 synthesized by photo-assisted deposition and impregnation methods, Journal of Materials Processing Technology 209(1) (2009) 577-583. https://doi.org/10.1016/j.jmatprotec.2008.02.027

[14] D. Wang, B. Yin, A. Sun, X. Li, C. Qi, B. Duan, Fabrication of Mo–Cu composite powders by heterogeneous precipitation and the sintering properties of the composite compacts, Journal of Alloys and Compounds 674 (2016) 347-352. https://doi.org/10.1016/j.jallcom.2016.03.027

[15] D. Wang, BangzhuSun, AokuiLi, XiulinQi, ChengkangDuan, Bohua, Fabrication of Mo-Cu composite powders by heterogeneous precipitation and the sintering properties of the composite compacts, Journal of Alloys and Compounds: An Interdisciplinary Journal of Materials Science and Solid-state Chemistry and Physics 674(Null) (2016).

[16] P. Song, J. Cheng, L. Wan, J. Zhao, Y. Wang, Y. Cai, Preparation and characterization of Mo-15 Cu superfine powders by a gelatification-reduction process, Journal of Alloys and Compounds 476(1) (2009) 226-230. https://doi.org/https://doi.org/10.1016/j.jallcom.2008.09.097

[17] R. Zheng, S.F. Li, R.D.K. Misra, K. Kondoh, Y.F. Yang, Role of W in W-coated Cu powder in enhancing the densification-conductivity synergy of laser powder bed fusion built Cu component, Journal of Materials Processing Technology 322 (2023) 118169. https://doi.org/10.1016/j.jmatprotec.2023.118169

[18] Y. Wang, M. Tayyebi, M. Tayebi, M. Yarigarravesh, S. Liu, H. Zhang, Effect

of whisker alignment on microstructure, mechanical and thermal properties of Mg-SiCw/Cu composite fabricated by a combination of casting and severe plastic deformation (SPD), Journal of Magnesium and Alloys 11(3) (2023) 966-980. https://doi.org/10.1016/j.jma.2022.11.004

[19] X. Guo, K. Duan, X. Wang, K. Song, X. Zhang, K. Li, Thermal and arc erosion behavior of CuCr contact material based on large plastic deformation treatment, Journal of Materials Research and Technology 23 (2023) 348-358. https://doi.org/10.1016/j.jmrt.2023.01.011

[20] X.J. Zheng, W.B. Fan, F. Xue, Effect of Different Blank Making Process on Microstructure and Properties of Rolled Mo-Cu Sheet, Nonferrous Metals Engineering 10(08) (2020) 1-4+9.

[21] J. Johnson, Role of solid-state skeletal sintering during processing of Mo-Cu composites, Metallurgical and Materials Transactions A 32 (2001) 605-613. https://doi.org/10.1007/s11661-001-0077-y

[22] J. Reiser, A. Hoffmann, J. Hain, U. Jäntsch, M. Klimenkov, J. Hohe, T. Mrotzek, Thermal management materials based on molybdenum (Mo) and copper (Cu): Elucidation of the rolling-induced evolution of thermo-physical properties (e.g. CTE), Journal of Alloys and Compounds 776 (2019) 387-416. https://doi.org/10.1016/j.jallcom.2018.10.235

[23] L. Wang, L. Xu, C. Srinivasakannan, S. Koppala, Z. Han, H. Xia, Electroless copper plating of tungsten powders and preparation of WCu20 composites by microwave sintering, Journal of Alloys and Compounds 764 (2018) 177-185. https://doi.org/10.1016/j.jallcom.2018.06.061

[24] H. Wang, F. Li, Y. Chen, C. Li, Z. Wang, Y. Huang, Improved strength and heat transfer of W/Cu joints via surface nano-activation of W, Fusion Engineering and Design 182 (2022) 113219. https://doi.org/10.1016/j.fusengdes.2022.113219

[25] Z. Niu, P. Wang, R. Ma, Z. Hao, Y. Shu, J. He, Microstructure, electrical conductivity and mechanical properties of CoCrFeNi-Cu composite, Materials Today Communications 36 (2023) 106762. https://doi.org/10.1016/j.mtcomm.2023.106762

[26] P. Chui, K. Sun, C. Sun, X. Yang, T. Shan, Effect of surface nanocrystallization induced by fast multiple rotation rolling on hardness and corrosion behavior of 316L stainless steel, Applied Surface Science 257(15) (2011) 6787-6791. https://doi.org/10.1016/j.apsusc.2011.02.127

[27] J. Li, K. Yamanaka, A. Chiba, Significant lattice-distortion effect on compressive deformation in Mo-added CoCrFeNi-based high-entropy alloys, Materials Science and Engineering: A 830 (2022) 142295. https://doi.org/10.1016/j.msea.2021.142295

[28] J. Lei, L. Ma, Z. Cai, W. Jia, Y. Yuan, H. Pan, H. Xie, Interfacial microstructure evolution for coordinated deformation of Mg/Al composite plates by asymmetrical rolling with differential temperature rolls, Journal of Magnesium and Alloys (2023). https://doi.org/10.1016/j.jma.2023.04.012

[29] W. Liao, H. Qiang, W. Song, Y. Hu, C. Zhang, Effect and mechanism of room temperature rolling, cryogenic rolling and heat treatment on mechanical properties and electrical conductivity of Cu-Ni-Si alloy with continuous directional

solidification, Journal of Alloys and Compounds 949 (2023) 169748. https://doi.org/10.1016/j.jallcom.2023.169748

[30] P.C. Maity, N.V. Pulagara, K.N. Chaithanya Kumar, I. Lahiri, K.S. Suresh, Stability and deviations from the cube texture during rolling and annealing of Ni foil, Materials Chemistry and Physics 297 (2023) 127326. https://doi.org/10.1016/j.matchemphys.2023.127326

[31] C. Maurice, J.H. Driver, Hot rolling textures of f.c.c. metals-part I. Experimental results on Al single And polycrystals, Acta Materialia 45(11) (1997) p.4627-4638.

[32] L.A.I. Kestens, H. Pirgazi, Texture formation in metal alloys with cubic crystal structures, Materials Science and Technology 32(13) (2016) 1303-1315. https://doi.org/10.1080/02670836.2016.1231746

[33] C.T. Zhi, L.F. Ma, Q.X. Huang, Y.C. Zhu, G.H. Zhao, Effect of cross rolling on microstructure and formability of AZ31B magnesium alloy edge, Rare Metal Materials and Engineering 47(05) (2018) 1555-1561.

[34] H. Sheng, Z. Sun, I. Uytdenhouwen, G. Van Oost, J. Vleugels, Temperature and deformation effect on the low and high angle grain boundary structure of a double forged pure tungsten, International Journal of Refractory Metals and Hard Materials 50 (2015) 184-190. https://doi.org/10.1016/j.ijrmhm.2015.01.008

[35] L. Dong, F. Yang, T. Yu, N. Zhang, X. Zhou, Z. Xie, F. Fang, Contribution of grain boundary to strength and electrical conductivity of annealed copper wires, Journal of Materials Research and Technology 26 (2023) 1459-1468. https://doi.org/10.1016/j.jmrt.2023.08.012

[36] R. Li, X. Chen, J. Wang, B. Li, F. Yan, G. Zhang, High-temperature compression behavior of bimodal α-Mo structured Mo-Si-B alloy, International Journal of Refractory Metals and Hard Materials 112 (2023) 106167. https://doi.org/10.1016/j.ijrmhm.2023.106167

[37] R. Han, G. Yang, Z. Fu, D. Xu, Y. Xu, G. Zhao, Effect of low-temperature hot rolling on the microstructure and mechanical properties of air-cooling medium manganese martensitic wear-resistant steel, Materials Characterization 203 (2023) 113139. https://doi.org/10.1016/j.matchar.2023.113139

[38] L. Hua, X. Hu, X. Han, Microstructure evolution of annealed 7075 aluminum alloy and its influence on room-temperature plasticity, Materials & Design 196 (2020) 109192. https://doi.org/10.1016/j.matdes.2020.109192

[39] J.Z. Wang, J.Q. Yin, J.W. Cui, J. Chang, Y.D. YU, Y.L. Sun, Intergranular Reaction Mechanism of Submicron-Activated Mo-15Cu Alloy, Rare Metal Materials and Engineering 52(02) (2023) 448-453.

[40] J.P. Hirth, J. Lothe, T. Mura, Theory of Dislocations (2nd ed.), Journal of Applied Mechanics 50(2) (1983) 476-477. https://doi.org/10.1115/1.3167075

[41] J.Y. Liu, L. Lu, Z.Y. Zhong, Deformation twins and annealing twins in high purity coarse-grained aluminum by equal channel angular pressing at high strain rate, Journal of Materials Engineering 49(04) (2021) 89-94.

[42] S. Mahajan, C.S. Pande, M.A. Imam, B.B. Rath, Formation of annealing twins in f.c.c. crystals, Acta Materialia 45(6) (1997) 2633-2638.

https://doi.org/https://doi.org/10.1016/S1359-6454(96)00336-9

[43] W. Wang, F. Brisset, A.L. Helbert, D. Solas, I. Drouelle, M.H. Mathon, T. Baudin, Influence of stored energy on twin formation during primary recrystallization, Materials Science and Engineering: A 589 (2014) 112-118. https://doi.org/10.1016/j.msea.2013.09.071

[44] D.P. Field, R.C. Eames, T.M. Lillo, The role of shear stress in the formation of annealing twin boundaries in copper, Scripta Materialia 54(6) (2006) 983-986. https://doi.org/10.1016/j.scriptamat.2005.11.037

[45] Y.L. Gong, C.E. Wen, X.X. Wu, S.Y. Ren, L.P. Cheng, X.K. Zhu, The influence of strain rate, deformation temperature and stacking fault energy on the mechanical properties of Cu alloys, Materials Science and Engineering: A 583 (2013) 199-204. https://doi.org/https://doi.org/10.1016/j.msea.2013.07.001

[46] N. Lugo, N. Llorca, J.M. Cabrera, Z. Horita, Microstructures and mechanical properties of pure copper deformed severely by equal-channel angular pressing and high pressure torsion, Materials Science and Engineering: A 477(1-2) (2008) 366-371. https://doi.org/10.1016/j.msea.2007.05.083

[47] J. Chen, X. Ma, W. Yan, F. Xia, X. Fan, Effect of Transverse Grain Boundary on Microstructure, Texture and Mechanical Properties of Drawn Copper Wires, Journal of Materials Science & Technology 30(2) (2014) 184-191. https://doi.org/https://doi.org/10.1016/j.jmst.2013.04.018

[48] E. Bringa, D. Farkas, A. Caro, Y. Wang, J. McNaney, R. Smith, Fivefold twin formation during annealing of nanocrystalline Cu, Scripta Materialia 59(12) (2008) 1267-1270. https://doi.org/10.1016/j.scriptamat.2008.08.041

[49] L. Murr, Interfacial Phenomena in Metals and Alloys, 1975.

[50] J. Wang, N. Li, O. Anderoglu, X. Zhang, A. Misra, J.Y. Huang, J.P. Hirth, Detwinning mechanisms for growth twins in face-centered cubic metals, Acta Materialia 58(6) (2010) 2262-2270. https://doi.org/10.1016/j.actamat.2009.12.013

[51] H.-Y. Yang, Z.-J. Cai, Q. Zhang, Y. Shao, B.-X. Dong, Q.-Q. Xuan, F. Qiu, Comparison of the effects of Mg and Zn on the interface mismatch and compression properties of 50 vol% TiB2/Al composites, Ceramics International 47(15) (2021) 22121-22129. https://doi.org/10.1016/j.ceramint.2021.04.234

[52] S.S.R. Pulagam, A. Dutta, Peierls–Nabarro modeling of twinning dislocations in fcc metals, Computational Materials Science 206 (2022) 111269. https://doi.org/10.1016/j.commatsci.2022.111269

[53] J.L. Dequiedt, Slip system interactions in BCC single crystals: System deactivation and segregation, Mechanics of Materials 184 (2023) 104730. https://doi.org/10.1016/j.mechmat.2023.104730

[54] R. Kositski, D. Mordehai, Role of dislocation pile-ups in nucleation-controlled size-dependent strength of Fe nanowires, Acta Materialia 136 (2017) 190-201. https://doi.org/10.1016/j.actamat.2017.06.057

[55] S. Jin, D. Zhang, X. Lu, Y. Zhang, L. Tan, Y. Liu, Q. Wang, Mechanical properties, biodegradability and cytocompatibility of biodegradable Mg-Zn-Zr-Nd/Y alloys, Journal of Materials Science & Technology 47 (2020) 190-201. https://doi.org/10.1016/j.jmst.2020.02.017

[56] B.N. Du, Z.Y. Hu, L.Y. Sheng, D.K. Xu, Y.X. Qiao, B.J. Wang, J. Wang, Y.F. Zheng, T.F. Xi, Microstructural characteristics and mechanical properties of the hot extruded Mg-Zn-Y-Nd alloys, Journal of Materials Science & Technology 60 (2021) 44-55. https://doi.org/10.1016/j.jmst.2020.05.021

[57] J. Li, R. Dong, H. Kou, J. Fan, B. Zhu, B. Tang, Texture evolution and the recrystallization behavior in a near β titanium alloy Ti-7333 during the hot-rolling process, Materials Characterization 159 (2020) 109999. https://doi.org/10.1016/j.matchar.2019.109999

[58] X.J. Zheng, W.B. Fan, F. Xue, Effect of different preforming processes on microstructure and properties of rolled molybdenum copper sheet, Nonferrous Metals Engineering 10(08) (2020) 1-4+9.

[59] C. Li, H. Hou, R. Dong, X. Zhang, X. Xu, Y. Zhao, Recrystallization behavior and mechanical properties of AZ31B alloy during the hot-rolling process, Journal of Materials Research and Technology 24 (2023) 1005-1014. https://doi.org/10.1016/j.jmrt.2023.02.133

[60] B.H. Duan, H.X. Hong, D.Z. Wang, H.J. Liu, C.G. Xie, S. Wang, Preparation of Mo-Cu alloy by gel injection infiltration method, Materials Science and Engineering of Powder Metallurgy 18(05) (2013) 729-734.

[61] V. Sinha, J.E. Spowart, Influence of interfacial carbide layer characteristics on thermal properties of copper–diamond composites, Journal of Materials Science 48(3) (2013) 1330-1341. https://doi.org/10.1007/s10853-012-6878-0

[62] A. Sun, Y. Liu, D. Wang, Z. Zhou, Sintering Behavior and Properties of Mo-Cu Composites, Advances in Materials Science and Engineering 2018 (2018) 8703986. https://doi.org/10.1155/2018/8703986

[63] D.-G. Kim, K.W. Lee, S.-T. Oh, Y.D. Kim, Preparation of W–Cu nanocomposite powder by hydrogen-reduction of ball-milled W and CuO powder mixture, Materials Letters 58(7-8) (2004) 1199-1203. https://doi.org/10.1016/j.matlet.2003.08.035

[64] Z. Cao, S. Chen, Z. Jiang, H. Chen, J. Sun, K. Jing, Q. Huang, J. Huang, Effect of Si-coated diamond on the relative density and thermal conductivity of diamond/W composites prepared by SPS, Vacuum 209 (2023) 111728. https://doi.org/10.1016/j.vacuum.2022.111728

[65] N. Al-Aqeeli, K. Abdullahi, A.S. Hakeem, C. Suryanarayana, T. Laoui, S. Nouari, Synthesis, characterisation and mechanical properties of SiC reinforced Al based nanocomposites processed by MA and SPS, Powder Metallurgy 56(2) (2013) 149-157. https://doi.org/10.1179/1743290112y.0000000029

[66] K.V. Reddy, S. Pal, Cold-rolling induced residual stress effect on the shock response of crystalline-metallic glass (Cu–CuZr) nanolaminates by molecular dynamics simulation, Materials Chemistry and Physics 272 (2021) 125010. https://doi.org/10.1016/j.matchemphys.2021.125010

[67] X.-Y. Tan, L.-M. Luo, Z.-L. Lu, G.-N. Luo, X. Zan, J.-G. Cheng, Y.-C. Wu, Development of tungsten as plasma-facing materials by doping tantalum carbide nanoparticles, Powder Technology 269 (2015) 437-442. https://doi.org/10.1016/j.powtec.2014.09.039

[68] X. Wang, X. Zhang, L. Zhao, C. Zhao, H. Zhang, Y. Du, W. Zhang, Y. Guo, P. Cao, Tungsten/copper composite sheets prepared by a novel encapsulation rolling technique, Journal of Alloys and Compounds 884 (2021) 161051. https://doi.org/10.1016/j.jallcom.2021.161051

[69] K. Euh, S.B. Kang, Effect of rolling on the thermo-physical properties of SiCp/Al composites fabricated by plasma spraying, Materials Science and Engineering: A 395(1-2) (2005) 47-52. https://doi.org/10.1016/j.msea.2004.12.051

[70] S. Miao, Z.M. Xie, X.D. Yang, R. Liu, R. Gao, T. Zhang, X.P. Wang, Q.F. Fang, C.S. Liu, G.N. Luo, X. Liu, Y.Y. Lian, Effect of hot rolling and annealing on the mechanical properties and thermal conductivity of W-0.5wt.% TaC alloys, International Journal of Refractory Metals and Hard Materials 56 (2016) 8-17. https://doi.org/10.1016/j.ijrmhm.2015.12.004

[71] O.V. Ogorodnikova, J. Roth, M. Mayer, Deuterium retention in tungsten in dependence of the surface conditions, Journal of Nuclear Materials 313-316 (2003) 469-477. https://doi.org/https://doi.org/10.1016/S0022-3115(02)01375-2

[72] D. Wang, X. Dong, P. Zhou, A. Sun, B. Duan, The sintering behavior of ultra-fine Mo–Cu composite powders and the sintering properties of the composite compacts, International Journal of Refractory Metals and Hard Materials 42 (2014) 240-245. https://doi.org/10.1016/j.ijrmhm.2013.09.012

[73] T.G. Wang, Q.C. Liang, Q. Qin, Preparation of Mo-Cu alloy by powder metallurgy and its properties, Materials Reports 29(10) (2015) 97-99.

[74] J.-T. Yao, C.-J. Li, Y. Li, B. Chen, H.-B. Huo, Relationships between the properties and microstructure of Mo–Cu composites prepared by infiltrating copper into flame-sprayed porous Mo skeleton, Materials & Design 88 (2015) 774-780. https://doi.org/10.1016/j.matdes.2015.09.062